Available online at www.sciencedirect.com
ScienceDirect
Journal of Computational Physics 223 (2007) 67–81
JOURNAL OF COMPUTATIONAL PHYSICS
www.elsevier.com/locate/jcp

Discontinuous Galerkin finite element method applied to the 1-D spherical neutron transport equation ☆

Eric Machorro *

Department of Applied Mathematics, University of Washington, P.O. Box 352420, 408 Gugenheim Hall, Seattle, WA 98195-2420, United States
Center for Applied Scientific Computing, Lawrence Livermore National Laboratory, P.O. Box 808 L-419, Livermore, CA 94551, United States

Received 10 November 2005; received in revised form 9 August 2006; accepted 26 August 2006
Available online 25 October 2006

Abstract

Discontinuous Galerkin finite element methods are used to estimate solutions to the non-scattering 1-D spherical neutron transport equation. Various trial and test spaces are compared in the context of a few sample problems whose exact solution is known. Certain trial spaces avoid unphysical behaviors that seem to plague other methods. Comparisons with diamond differencing and simple corner-balancing are presented to highlight these improvements.

Keywords: Linear hyperbolic equation; Neutron transport; Finite elements; Corner balance method; Diamond difference method; Discontinuous Galerkin methods; Spherical geometry Sn equations

1. Introduction

On a domain $\mathscr{D} = [0,1] \times [-1,1]$ in *non-dimensionalized* (r,μ) space, the conservative form of the 1-D spherical neutron transport equation is given in [12] by

$$\frac{\mu}{r^2}\frac{\partial}{\partial r}(r^2\psi) + \frac{\partial}{\partial \mu}\left(\frac{1-\mu^2}{r}\psi\right) + \sigma(r,\mu)\psi = q \tag{1.1}$$

where the cross-section and source terms are nonnegative: $\sigma, q \geqslant 0$. Vacuum boundary conditions are taken to be the condition that $\psi(1, \mu \leqslant 0) = 0$.

Sections 2–4 of this paper introduce respectively the diamond difference (DD), discontinuous Galerkin (DG) finite element and simple corner balance (SCB) methods considered. Sections 5 and 6 present the test problems and related numerical results. Conclusions are drawn in Section 7.

☆ This work was supported in part by DOE grant DE-FG02-03ER25576. Review & Release UCRL-JRNL-216956.
* Address: Center for Applied Scientific Computing, Lawrence Livermore National Laboratory, P.O. Box 808 L-419, Livermore, CA 94551, United States. Tel.: +1 503 449 0686.
E-mail addresses: machorro@amath.washington.edu, machorro2@llnl.gov.

0021-9991/$ - see front matter © 2006 Elsevier Inc. All rights reserved.
doi:10.1016/j.jcp.2006.08.020

1.1. Criteria

The following criteria are commonly used in deciding which numerical method might be used in solving the neutron transport equation.

1. *Positivity*: Given nonnegative boundary conditions, cross-section σ, and source q, the true solution will be nonnegative. The numerical method should also yield a nonnegative solution. This avoids unphysical oscillations and the need for unreliable zero-flux fix-ups. This problem tends to crop up especially in the vicinity of material interfaces (discontinuities in σ or q).
2. *Avoids flux 'dip' near the origin*: Due to the singular nature of (1.1) near $r = 0$, many methods exhibit an aberrant numerical 'dip' in the neutron flux calculation that is not physical. This is especially problematic as that region is often the primary area of scientific interest.
3. *Convergence*: This is closely related to overall accuracy and computational efficiency but is measured here by the reduction in error as the mesh size is decreased. Although the local truncation error can, for many methods, be shown to be second order, the global error is often lower order due to the discontinuous derivatives that are inherent in many solutions to problems of scientific interest. Even in some very simple cases, the true solution lacks smooth partial derivatives – see Section 5.2.
4. *Computational cost*: This is roughly measured in the number of arithmetic operations (flops) required per cell. This can be difficult to precisely compare from one method to another, as flop counts can vary considerably from one implementation of an algorithm to another implementation of the same algorithm.

Another common requirement of a numerical method is conservation. Since all methods considered here are unequivocally conservative, any comparison based on that criterion is omitted here in the interest of brevity.

1.2. Mesh

A mesh dividing the domain $\mathscr{D} = [0,1] \times [-1,1]$ in (r,μ) space with n_r radial zones $\left\{\left[r_{i-\frac{1}{2}}, r_{i+\frac{1}{2}}\right]\right\}_{i=1}^{n_r}$ and n_μ angles is used. Half-indices in the radial direction are interpreted as $r_{i+\frac{1}{2}} = r_i + \Delta r_i/2$. However, angular discretization is slightly different from one method to the next. In the diamond difference, weighted diamond

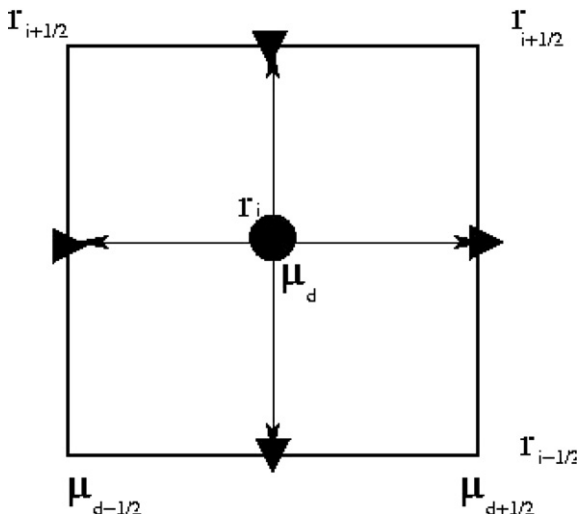

Fig. 1.1. A cell $C_{i,d} = \left[r_{i-\frac{1}{2}}, r_{i+\frac{1}{2}}\right] \times \left[\mu_{d-\frac{1}{2}}, \mu_{d+\frac{1}{2}}\right]$ (alternatively referred to as a corner or subcell) with center r_i, μ_d. In DD based methods, the center-value $\psi_{i,d}$ is the average of both pairs of opposing edges as described by (2.2) and (2.3) with the upstream edge determined by the value of μ_d. Here, the larger arrows indicate the characteristic direction associated with $\mu_d < 0$.

difference and simple corner balance methods, $\mu_{\frac{1}{2}} = -1$ and $\mu_{d+\frac{1}{2}} = \mu_{d-\frac{1}{2}} + w_d$ for $\{w_d\}$, the set of Gauss Legendre quadrature weights. This leads to a collection of cell edges with the interesting property that

$$-1 = \mu_{\frac{1}{2}} < \mu_1 < \cdots < \mu_{d-\frac{1}{2}} < \mu_d < \mu_{d+\frac{1}{2}} < \cdots < \mu_{n_\mu} < \mu_{n_\mu+\frac{1}{2}} = 1$$

where $\{\mu_d\}_{d=1}^{n_\mu}$ is the set of n_μ Gauss–Legendre points on the interval $[-1,1]$ associated with the quadrature weights $\{w_d\}$.

For the various discontinuous Galerkin (DG) methods considered here, angular cell edge values $\mu_{d+\frac{1}{2}}$ are the same as in the diamond difference method. However,

$$(\mu_d)_{\mathrm{DG}} = \frac{\mu_{d-\frac{1}{2}} + \mu_{d+\frac{1}{2}}}{2}.$$

where the context is clear, the subscript DG above will be dropped. In the presentation that follows, it is often assumed that q and σ are piecewise constant.

It will be convenient to define a cell (Fig. 1.1),

$$C_{i,d} = \left[r_{i-\frac{1}{2}}, r_{i+\frac{1}{2}}\right] \times \left[\mu_{d-\frac{1}{2}}, \mu_{d+\frac{1}{2}}\right] \tag{1.2}$$

and use the terms cell, subcell and corner interchangeably. In Section 4, the definition of a macrocell is introduced. It is distinct from the definition above.

Formally, a mesh $\mathscr{M}$ is the collection of cells,

$$\mathscr{M} = \{C_{i,d} : 1 \leqslant i \leqslant n_{\mathrm{r}} \text{ and } 1 \leqslant d \leqslant n_\mu\}.$$

2. Diamond difference method

The diamond difference method (DD) is a common technique for solving the neutron transport equation, and it is well described in the literature. In particular, [12] has an extensive description. To balance clarity with brevity however, the basic equations of the DD method are presented here with only a brief exposition.

Taking Eq. (1.1) with $\mu = \mu_d$ and integrating over the volume V_i of the spherical shell of radius bounded by $r_{i-\frac{1}{2}}$ and $r_{i+\frac{1}{2}}$ we arrive at

$$\frac{\mu_d}{V_i}\left(A_{i+\frac{1}{2}}\psi_{i+\frac{1}{2},d} - A_{i-\frac{1}{2}}\psi_{i-\frac{1}{2},d}\right) + \frac{\Delta A_i}{w_d V_i}\left(\alpha_{d+\frac{1}{2}}\psi_{i,d+\frac{1}{2}} - \alpha_{d-\frac{1}{2}}\psi_{i,d-\frac{1}{2}}\right) + \sigma\psi_{i,d} = q_{i,d} \tag{2.1}$$

for $A_{i+\frac{1}{2}} = 4\pi r_{i+\frac{1}{2}}^2$, $\Delta A_i = A_{i+\frac{1}{2}} - A_{i-\frac{1}{2}}$ and angular differencing coefficients $\alpha_{d+\frac{1}{2}} = \alpha_{d-\frac{1}{2}} - \mu_d w_d$ chosen to maintain conservation properties. Note that $V_i = \frac{4\pi}{3}\left(r_{i+\frac{1}{2}}^3 - r_{i-\frac{1}{2}}^3\right)$. The approximation

$$4\pi \int_{r_{i-\frac{1}{2}}}^{r_{i+\frac{1}{2}}} r\psi(r,\mu_d)\,\mathrm{d}r \approx \frac{1}{2}\left(A_{i+\frac{1}{2}} - A_{i-\frac{1}{2}}\right)\psi_{i,d}$$

is also used in deriving (2.1) from (1.1).

As auxiliary equations, the DD method assumes that cell edges are "averaged" across the interior of the cell, in that

$$\psi_{i,d} = \frac{\psi_{i+\frac{1}{2},d} + \psi_{i-\frac{1}{2},d}}{2} \quad \text{and} \tag{2.2}$$

$$\psi_{i,d} = \frac{\psi_{i,d+\frac{1}{2}} + \psi_{i,d-\frac{1}{2}}}{2}. \tag{2.3}$$

2.1. Weighted diamond difference equations

The weighted diamond difference (WDD) method was introduced in [14] in an effort to remove certain spurious unphysical artifacts that seemed to plague the DD method (see Section 6.3). The method is based on the DD balance equation (2.1), but uses modified auxiliary relations, replacing the auxiliary equation (2.3) with a weighted average

$$\psi_{i,d} = \tau_d \psi_{i,d+\frac{1}{2}} + (1-\tau_d)\psi_{i,d-\frac{1}{2}} \tag{2.4}$$

for angular differencing weights $\{\tau_d\}_{d=1}^{n_\mu}$ defined by

$$\tau_d = \frac{\mu_d - \mu_{d-\frac{1}{2}}}{\mu_{d+\frac{1}{2}} - \mu_{d-\frac{1}{2}}}. \tag{2.5}$$

It should be noted that the angular-discretization ideas of [14] can be incorporated into other schemes for radial discretization. In fact, Walters and Morel in [17] incorporate a radial discontinuous Galerkin method with a WDD angular-discretization scheme, and report some success when the angular mesh is poorly resolved. See Section 6.3 for further discussion.

3. Discontinuous Galerkin finite element method

Discontinuous finite element methods have long been applied to neutron transport problems in a variety of different settings, for example [1,4,6,8,10] among many others. This particular geometry has not been as extensively studied in the literature, however, with [15–17] being the only recent references on the subject known to this author.

It is easiest to introduce the discontinuous Galerkin (DG) finite element method in the following four parts:

1. *The Weak form* of the transport equation is said to hold if ψ satisfies
$$\int_{r_{i-\frac{1}{2}}}^{r_{i+\frac{1}{2}}}\int_{\mu_{d-\frac{1}{2}}}^{\mu_{d+\frac{1}{2}}} r^2\left(\frac{\mu}{r^2}\frac{\partial}{\partial r}(r^2\psi) + \frac{\partial}{\partial \mu}\left(\frac{1-\mu^2}{r}\psi\right)\right)\tau\,\mathrm{d}\mu\,\mathrm{d}r + \int_{r_{i-\frac{1}{2}}}^{r_{i+\frac{1}{2}}}\int_{\mu_{d-\frac{1}{2}}}^{\mu_{d+\frac{1}{2}}} r^2(\sigma(r,\mu)\psi - q)\tau\,\mathrm{d}\mu\,\mathrm{d}r = 0 \tag{3.1}$$
for all cells $C_{i,d} = \left[r_{i-\frac{1}{2}}, r_{i+\frac{1}{2}}\right] \times \left[\mu_{d-\frac{1}{2}}, \mu_{d+\frac{1}{2}}\right]$, and all test functions $\tau(r,\mu)$ in an appropriate function space as described below. See also [7].
2. *Test functions:* The main test spaces being considered here are the sets of $\tau \in K_{i,d}$ where $K_{i,d}$ is one of the following polynomial spaces:
$$\mathrm{DG}_{\mathrm{step}} : K_{i,d} = \mathrm{span}\{1\} \tag{3.2}$$
$$\mathrm{DG}_{\mathrm{bilinear}} : K_{i,d} = \mathrm{span}\{1, (r-r_i), (\mu-\mu_d), (r-r_i)(\mu-\mu_d)\} \tag{3.3}$$
for (r_i, μ_d) the cell center. Other test function spaces are also considered, some of which are discussed here in Section 6 and in [15].
3. *Trial functions:* Within a given cell, the approximate solution $\psi_{\mathrm{est}}(r,\mu)$ is represented also as a member of the set $K_{i,d}$. As an example, for appropriately chosen constants $\{\gamma_{i,d}^{(0,0)}, \gamma_{i,d}^{(1,0)}, \gamma_{i,d}^{(0,1)}, \gamma_{i,d}^{(1,1)}\}$, the $\mathrm{DG}_{\mathrm{bilinear}}$ method estimates ψ by the following:
$$\psi_{\mathrm{est}}(r,\mu) = \sum_{a,b=0}^{1} \gamma_{i,d}^{(a,b)}(r-r_i)^a(\mu-\mu_d)^b \in K_{i,d} \tag{3.4}$$
for $(r,\mu) \in \left[r_{i-\frac{1}{2}}, r_{i+\frac{1}{2}}\right] \times \left[\mu_{d-\frac{1}{2}}, \mu_{d+\frac{1}{2}}\right]$. The constants are determined from the weak form of Eq. (3.1).
4. *Cell edges:* Receive/transmit boundary information in the characteristic direction (depending on μ) to and from adjoining cells vis-a-vis integration by parts applied to (3.1)
$$\begin{aligned}
&\int_{\mu_{d-\frac{1}{2}}}^{\mu_{d+\frac{1}{2}}} \mu r^2\psi(r,\mu)\tau(r,\mu)\Big|_{r_{i-\frac{1}{2}}}^{r_{i+\frac{1}{2}}}\mathrm{d}\mu + \int_{r_{i-\frac{1}{2}}}^{r_{i+\frac{1}{2}}} r(1-\mu^2)\psi(r,\mu)\tau(r,\mu)\Big|_{\mu_{d-\frac{1}{2}}}^{\mu_{d+\frac{1}{2}}}\mathrm{d}r \\
&\quad - \int_{r_{i-\frac{1}{2}}}^{r_{i+\frac{1}{2}}}\int_{\mu_{d-\frac{1}{2}}}^{\mu_{d+\frac{1}{2}}}\left(\mu r^2\psi(r,\mu)\frac{\partial}{\partial r}\tau(r,\mu) + r(1-\mu^2)\psi(r,\mu)\frac{\partial}{\partial \mu}\tau(r,\mu)\right)\mathrm{d}\mu\,\mathrm{d}r \\
&\quad + \int_{r_{i-\frac{1}{2}}}^{r_{i+\frac{1}{2}}}\int_{\mu_{d-\frac{1}{2}}}^{\mu_{d+\frac{1}{2}}} r^2(\sigma(r,\mu)\psi(r,\mu) - q(r,\mu))\tau(r,\mu)\,\mathrm{d}\mu\,\mathrm{d}r = 0
\end{aligned} \tag{3.5}$$

In order for (3.1) to hold for all $\tau \in K_{i,d}$, it is sufficient to consider only the basis functions that generate $K_{i,d}$. The bilinear case is worked out in more detail below.

3.1. Bilinear discontinuous Galerkin

In the bilinear case ($DG_{bilinear}$), we need only consider the following test functions:

$$\tau(r,\mu) = 1, (r-r_i), (\mu-\mu_d), \quad \text{and} \quad (r-r_i)(\mu-\mu_d)$$

where in the cell $C_{i,d}$, the estimated solution ψ_{est} consequently has the form

$$\psi_{est}(r,\mu) = \gamma_{i,d}^{(0,0)} + \gamma_{i,d}^{(1,0)}(r-r_i) + \gamma_{i,d}^{(0,1)}(\mu-\mu_d) + \gamma_{i,d}^{(1,1)}(r-r_i)(\mu-\mu_d).$$

Solving for the coefficients $\{\gamma_{i,d}^{(a,b)}\}_{a,b=0}^{1}$ in (3.4) yields four (linear) equations relating the four unknowns. Even though these equations are based in the cell $C_{i,d}$, it is important to note that following the characteristic "flow" of information,

$$\psi\left(r,\mu_{d-\frac{1}{2}}\right) = \sum_{a,b=0}^{1} \gamma_{i,d-1}^{(a,b)}(r-r_i)^a\left(\mu_{d-\frac{1}{2}}-\mu_{d-1}\right)^b \tag{3.6}$$

$$\psi\left(r_{i+\frac{1}{2}},\mu\right) = \sum_{a,b=0}^{1} \gamma_{i+1,d}^{(a,b)}\left(r_{i+\frac{1}{2}}-r_{i+1}\right)^a(\mu-\mu_d)^b \tag{3.7}$$

for $\mu \leqslant 0$. This is *extremely* important in properly calculating the boundary terms in (3.5). For $\mu > 0$, (3.7) is replaced with

$$\psi\left(r_{i-\frac{1}{2}},\mu\right) = \sum_{a,b=0}^{1} \gamma_{i-1,d}^{(a,b)}\left(r_{i-\frac{1}{2}}-r_{i-1}\right)^a(\mu-\mu_d)^b. \tag{3.8}$$

3.2. Constant DG method DG_{step}

In the discontinuous Galerkin method DG_{step}, the trial and test function spaces are all piecewise constants. $K_{i,d} = \text{span}\{1\}$. Therefore, $\partial_\mu \tau = \partial_r \tau = 0$. This remarkably simplifies the weak form of the equation by reducing (3.5) to the equation

$$\int_{\mu_{d-\frac{1}{2}}}^{\mu_{d+\frac{1}{2}}} \mu r^2 \psi(r,\mu)\Big|_{r_{i-\frac{1}{2}}}^{r_{i+\frac{1}{2}}} \mathrm{d}\mu + \int_{r_{i-\frac{1}{2}}}^{r_{i+\frac{1}{2}}} r(1-\mu^2)\psi(r,\mu)\Big|_{\mu_{d-\frac{1}{2}}}^{\mu_{d+\frac{1}{2}}} \mathrm{d}r + \int_{r_{i-\frac{1}{2}}}^{r_{i+\frac{1}{2}}} \int_{\mu_{d-\frac{1}{2}}}^{\mu_{d+\frac{1}{2}}} r^2(\sigma(r,\mu)\psi(r,\mu) - q(r,\mu))\,\mathrm{d}\mu\,\mathrm{d}r = 0 \tag{3.9}$$

The boundary terms are evaluated using upstream information, and since

$$\psi|_{C_{i,d}}(r,\mu) = \gamma_{i,d}^{0,0}$$

the method requires that

$$\psi\left(r,\mu_{d-\frac{1}{2}}\right) = \gamma_{i,d-1}^{(0,0)} \tag{3.10}$$

and

$$\begin{aligned} &\psi\left(r_{i+\frac{1}{2}},\mu\right) = \gamma_{i+1,d}^{(0,0)} \quad \text{if } \mu < 0 \text{ else} \\ &\psi\left(r_{i-\frac{1}{2}},\mu\right) = \gamma_{i-1,d}^{(0,0)} \quad \text{when } \mu > 0 \end{aligned} \tag{3.11}$$

4. Simple corner balance method

Adapting the Cartesian corner-balance method in [2,3] to the spherically symmetric neutron Eq. (1.1) as in [16], it is convenient to think of a block of four adjoining cells with corresponding cell centers (r_{2i}, μ_{2d}),

(r_{2i-1}, μ_{2d}), (r_{2i-1}, μ_{2d-1}) and (r_{2i}, μ_{2d-1}), as a single macrocell, where each "subcell" or "corner" has a slightly different set of auxiliary relationships with its neighbors. To be precise, a macrocell denoted $M_{i,d}$ consists of the following cells:

$$M_{i,d} = C_{2i,2d} \cup C_{2i-1,2d} \cup C_{2i-1,2d-1} \cup C_{2i-1,2d-1} \tag{4.1}$$

This method requires both n_r and n_μ to be even. It is important to note the distinction between a subcell defined by (1.2) and the definition of a macrocell above (4.1).

The main balance equations from the DD method (2.1) are used within each sub-cell. In the case that $\mu < 0$, the following auxiliary relations are used. Starting with the known or previously calculated upstream "inherited" data that "flows" into the macro cell

$$\begin{aligned}
&\psi_{2i+\frac{1}{2},2d} \equiv \psi_{2i+1,2d} \\
&\psi_{2i+\frac{1}{2},2d-1} \equiv \psi_{2i+1,2d-1} \\
&\psi_{2i,2d-\frac{3}{2}} \equiv \psi_{2i,2d-2}, \quad \text{and} \\
&\psi_{2i-1,2d-\frac{3}{2}} \equiv \psi_{2i-1,2d-2} \quad \text{for } -1 < \mu_{2d} < 0.
\end{aligned} \tag{4.2}$$

Recall that it is assumed for illustrative purposes that $\mu_{2d} < 0$ and therefore the characteristic direction is radially inward. Internal to the macrocell are four more auxiliary equations that "take averages" across adjoining sub-cells within a given macrocell

$$\begin{aligned}
\psi_{2i-1,2d-\frac{1}{2}} &= \frac{1}{2}(\psi_{2i-1,2d} + \psi_{2i-1,2d-1}) \\
\psi_{2i-\frac{1}{2},2d} &= \frac{1}{2}(\psi_{2i,2d} + \psi_{2i-1,2d}) \\
\psi_{2i,2d-\frac{1}{2}} &= \frac{1}{2}(\psi_{2i,2d} + \psi_{2i,2d-1}) \\
\psi_{2i-\frac{1}{2},2d-1} &= \frac{1}{2}(\psi_{2i,2d-1} + \psi_{2i-1,2d-1}).
\end{aligned} \tag{4.3}$$

The mesh described by these points is illustrated in Fig. 4.1.

Through direct algebraic substitution and manipulation we arrive at four linear equations in the four unknown corner/sub-cell values

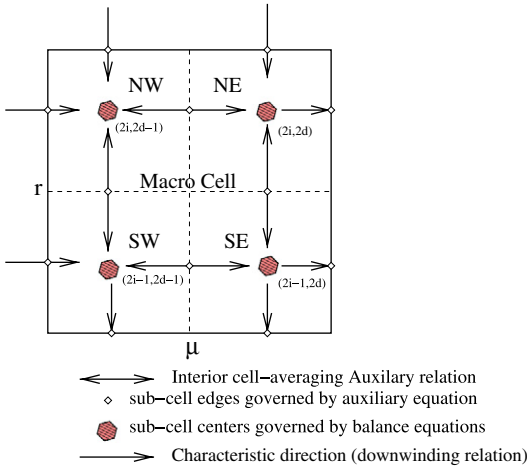

Fig. 4.1. This is a macrocell consisting of 4 subcells or corners: $C_{2i,2d}$, $C_{2i-1,2d}$, $C_{2i-1,2d-1}$ and $C_{2i,2d-1}$. Downwind/characteristic direction corresponding to $\mu < 0$. See (4.4)–(4.7) for the associated equations.

$$\frac{\mu_{2d}}{V_{2i}}\left(A_{2i+\frac{1}{2}}\psi_{2i+1,2d}-A_{2i-\frac{1}{2}}\frac{1}{2}(\psi_{2i,2d}+\psi_{2i-1,2d})\right)+\frac{\Delta A_{2i}}{w_{2d}V_{2i}}\left(\alpha_{2d+\frac{1}{2}}\psi_{2i,2d}-\alpha_{2d-\frac{1}{2}}\frac{1}{2}(\psi_{2i,2d}+\psi_{2i,2d-1})\right)+\sigma\psi_{2i,2d}=q_{2i,2d} \tag{4.4}$$

$$\frac{\mu_{2d}}{V_{2i-1}}\left(A_{2i-\frac{1}{2}}\frac{1}{2}(\psi_{2i,2d}+\psi_{2i-1,2d})-A_{2i-\frac{3}{2}}\psi_{2i-1,2d}\right)+\frac{\Delta A_{2i-1}}{w_{2d}V_{2i-1}}\left(\alpha_{2d+\frac{1}{2}}\psi_{2i-1,2d}-\alpha_{2d-\frac{1}{2}}\frac{1}{2}(\psi_{2i-1,2d}+\psi_{2i-1,2d-1})\right)+\sigma\psi_{2i-1,2d}=q_{2i-1,2d} \tag{4.5}$$

$$\frac{\mu_{2d-1}}{V_{2i-1}}\left(A_{2i-\frac{1}{2}}\frac{1}{2}(\psi_{2i,2d-1}+\psi_{2i-1,2d-1})-A_{2i-\frac{3}{2}}\frac{1}{2}\psi_{2i-1,2d-1}\right)+\frac{\Delta A_{2i-1}}{w_{2d-1}V_{2i-1}}\left(\alpha_{2d-\frac{1}{2}}\frac{1}{2}(\psi_{2i-1,2d}+\psi_{2i-1,2d-1})-\alpha_{2d-\frac{3}{2}}\psi_{2i-1,2d-2}\right)+\sigma\psi_{2i-1,2d-1}=q_{2i-1,2d-1} \tag{4.6}$$

$$\frac{\mu_{2d-1}}{V_{2i}}\left(A_{2i+\frac{1}{2}}\psi_{2i+1,2d-1}-A_{2i-\frac{1}{2}}\frac{1}{2}(\psi_{2i,2d-1}+\psi_{2i-1,2d-1})\right)+\frac{\Delta A_{2i}}{w_{2d-1}V_{2i}}\left(\alpha_{2d-\frac{1}{2}}\frac{1}{2}(\psi_{2i,2d}+\psi_{2i,2d-1})-\alpha_{2d-\frac{3}{2}}\psi_{2i,2d-2}\right)+\sigma\psi_{2i,2d-1}=q_{2i,2d-1} \tag{4.7}$$

5. Example problems

It should be emphasized that all the test problems considered here are limited in that they contain neither scattering nor fission terms. In a more realistic setting the right-hand side of (1.1) might have a more complicated expression of the form

$$q(r,\mu,\psi)=f(r,\mu)+\int_{-1}^{+1}k(r,\mu,\mu')\psi(r,\mu')\,\mathrm{d}\mu'$$

However, it is the intent of this article to focus only on discretizations of the streaming-plus-collision part of the transport operator as expressed by the left-hand side of (1.1). Therefore, $k\equiv 0$ is assumed here, although [14,15,17] consider the more common case where $k(r,\mu,\mu')\equiv\frac{1}{2}\sigma_s(r)$ for appropriate scattering coefficient σ_s with $\sigma-\sigma_s\geqslant 0$.

5.1. Smooth solutions and the method of manufactured solutions

Picking $\psi_{\text{true}}=\exp(r\mu)$ and adjusting σ, q and the boundary conditions to obey (1.1), an artificial, smooth solution can be "found" or manufactured. For instance,

$$\begin{aligned}\psi(r,\mu)&=\mathrm{e}^{r\mu}\\ q(r,\mu)&=2\mathrm{e}^{r\mu}\\ \sigma&=1.\end{aligned} \tag{5.1}$$

This is an artificial test problem of little practical value. It is being used here for the purpose of comparing convergence rates using a solution that has a full set of derivatives. This is in contrast to typical situations that arise such as described in Section 5.2.

Many other manufactured solutions can be produced in this manner to test these methods. Some are better than others for comparison purposes. Of course if $\psi_{\text{true}}|_{C_{i,d}}\in K_{i,d}$ for all i,d then the corresponding DG method will solve the neutron transport equation exactly. For example, if $\psi=r\mu+1$, then $\mathrm{DG}_{\text{bilinear}}$ will solve (1.1) exactly. This would be an unfair test problem to compare with other methods, although it may be helpful as a programming tool in double-checking and debugging.

5.2. Absorbing media test problems

Two test problems are considered here, both of which are described in [9]. The function

$$\psi(r,\mu) = \frac{q}{\sigma}\left(1 - e^{-\sigma\left(r\mu+\sqrt{1-r^2(1-\mu^2)}\right)}\right) \tag{5.2}$$

is the solution to the transport Eq. (1.1) with vacuum boundary conditions where both the source term (q) and the cross-section (σ) are constant. It is interesting to note that

$$\partial_r\psi(r,\mu) = q\left(e^{-\sigma(r\mu+\sqrt{1-r^2(1-\mu^2)})}\right)\left(\mu - \frac{r(1-\mu^2)}{\sqrt{1-r^2(1-\mu^2)}}\right) \tag{5.3}$$

and that on the curve

$$\sqrt{1-r^2(1-\mu^2)} = 0$$

the derivative is infinite. In particular, at the point $r = 1$, $\mu = 0$ the derivative is infinite and can cause $\partial_r\phi(1) = -\infty$ where ϕ is the scalar flux defined by (6.1).

The standard method of estimating error rates based on local truncation errors is founded on the assumption that the true solution has a full set of continuous derivatives. This is not the case here, even though it is one of the simplest non-trivial test problems conceivable. Therefore, there is no *prima facie* reason to think that commonly believed "second-order" numerical methods will have second order accuracy when used to solve these types of problems. Theoretical error estimates in a cylindrical geometry have been discussed in [4]. Carlson et al. in [5] also discuss error estimates under certain conditions.

Problems where there are two distinct regions each with separate material properties are modeled as follows (r_{mid} is the location of material boundary)

$$\sigma(r) = \begin{cases} \sigma_1 & \text{if } 0 \leqslant r < r_{\text{mid}}, \text{ or} \\ \sigma_2 & \text{if } r_{\text{mid}} \leqslant r \leqslant r_{\max} \end{cases}, \quad q(r) = \begin{cases} q_1 & \text{if } 0 \leqslant r < r_{\text{mid}}, \text{ or} \\ q_2 & \text{if } r_{\text{mid}} \leqslant r \leqslant r_{\max} \end{cases} \tag{5.4}$$

See Fig. 5.1. The solution is a bit more complicated than in the single-region case (5.2). For purposes of completeness, the explicit solution is given here but can also be found in [9].

When $0 \leqslant r \leqslant r_{\text{mid}}$ then

$$\psi(r,\mu) = \frac{q_1}{\sigma_1}(1 - e^{-\sigma_1(r\mu+s)}) + \frac{q_2}{\sigma_2}e^{(\sigma_2-\sigma_1)s-\sigma_1 r\mu}(e^{-\sigma_2 s} - e^{-\sigma_2 t}) \tag{5.5}$$

When $r_{\text{mid}} \leqslant r \leqslant 1$ and $-1 \leqslant \mu \leqslant \sqrt{1-(r_{\text{mid}}/r)^2}$ then

$$\psi(r,\mu) = \frac{q_2}{\sigma_2}(1 - e^{-\sigma_2(r\mu+t)}). \tag{5.6}$$

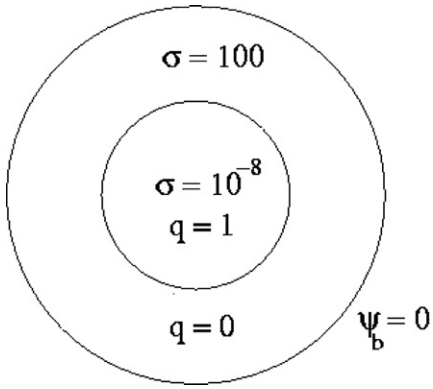

Fig. 5.1. Parameters used in Type (ii) test problem described by (5.4)–(5.7). A neutron source "region", encased by an outer strongly absorbing "shielding" region. The outer boundary is at $r = 1$. Vacuum boundary conditions are given as $\psi(1,\mu) = \psi_b = 0$ for $\mu \leqslant 0$. The interface between the two regions is at $r_{\text{mid}} = .4$.

When $r_{\text{mid}} \leqslant r \leqslant 1$ and $\sqrt{1-(r_{\text{mid}}/r)^2} \leqslant \mu \leqslant 1$,

$$\psi(r,\mu) = \frac{q_1}{\sigma_1} e^{\sigma_2 s - \sigma_2 r\mu}(1 - e^{-2\sigma_1 s}) + \frac{q_2}{\sigma_2} e^{2(\sigma_2-\sigma_1)s - \sigma_2 r\mu}(e^{-\sigma_2 s} - e^{-\sigma_2 t}) + \frac{q_2}{\sigma_2}(1 - e^{-\sigma_2(r\mu - s)}). \tag{5.7}$$

In these Eqs. 5.5, 5.6, and 5.7, the distances s and t are given by

$$s = \sqrt{r_{\text{mid}}^2 - r^2(1-\mu^2)} \quad \text{and,}$$
$$t = \sqrt{1 - r^2(1-\mu^2)}.$$

The following two sets of parameters are used to compare the various methods:

i. Test problem whose solution is given by (5.2) where $\sigma = q = 1$.
ii. Test problem given by the solution of (1.1) with (5.4)–(5.7) described by

$$r_{\text{mid}} = .4, \quad \sigma_1 = 10^{-8}, \quad \sigma_2 = 100, \quad q_1 = 1, \quad \text{and} \quad q_2 = 0$$

6. Results and comparisons

The scalar flux is defined as

$$\phi(r) = \int_{-1}^{+1} \psi(r,\mu)\, d\mu. \tag{6.1}$$

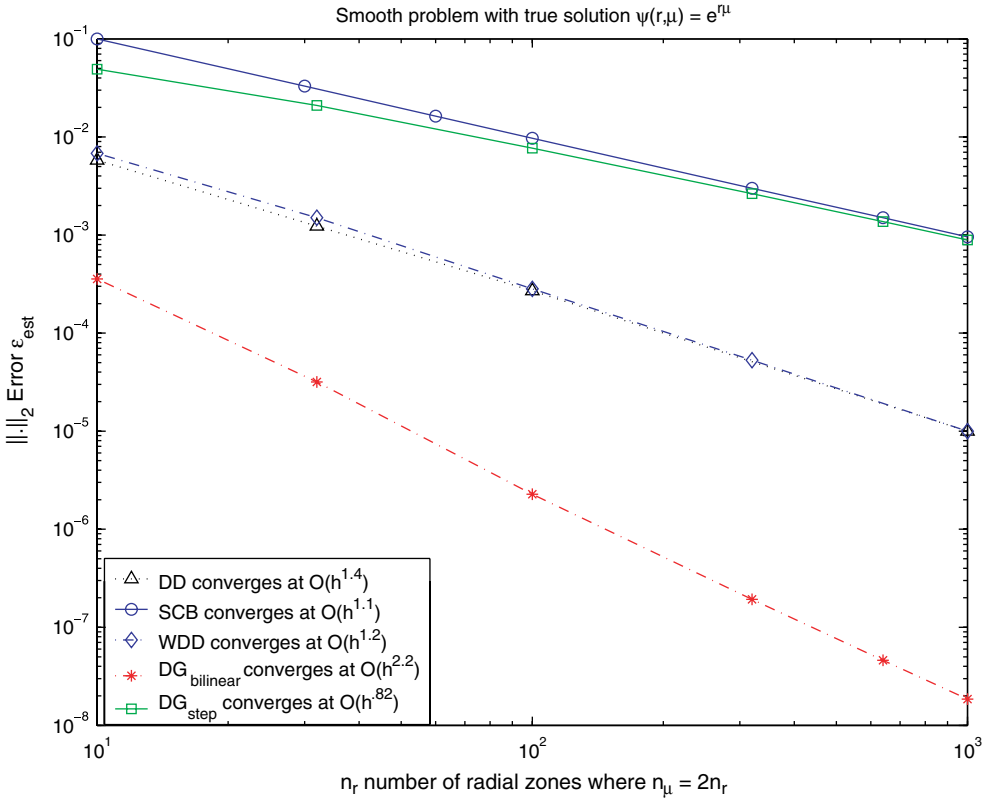

Fig. 6.1. $\|.\|_2$ error as function of the number of radial zones, n_r. The true solution, $\psi(r,\mu) = e^{r\mu}$, has well-defined derivatives of all orders. This is a test problem presented to showcase convergence properties. The vertical axis is ε_{est}, the L_2 error of the neutron flux defined by (6.2). The horizontal axis is n_r, depicting the increasing resolution of the mesh where the number of angular nodes is twice the number of radial nodes: $n_\mu = 2n_r$. In the legend, $h = \frac{1}{n_r}$.

It is frequently convenient to present numerical results using the scalar flux defined by (6.1) as in Figs. 6.3 and 6.4. Quadrature is used to calculate the integral quantities whereby

$$\phi_i = \sum_{d=1}^{d=n_\mu} \psi_{i,d} \Delta\mu_d$$

However when errors are reported such as in Figs. 6.1 and 6.2, the following L_2 based norm is used

$$\varepsilon_{\text{est}} = \sqrt{\sum_{i=1}^{n_r} \sum_{d=1}^{n_\mu} r_i^2 (\psi_{\text{exact}}(r_i, \mu_d) - \psi_{i,d}^{\text{est}})^2 \Delta r_i \Delta\mu_d} \tag{6.2}$$

6.1. Convergence

It is interesting to note in Figs. 6.1 and 6.2, that the $\text{DG}_{\text{bilinear}}$ method generally has better convergence than the SCB, WDD, DG_{step} or DD methods. Even in the case where the error rate is comparable (i.e. as in Fig. 6.2 the slopes of the lines are not very different), the actual error in the $\text{DG}_{\text{bilinear}}$ method is often less than the SCB and DG_{step} methods by a factor of 10 to 100. The higher accuracy may outweigh the substantially lower computation costs of the SCB method. See Table 6.1 in Section 7.

With the exception of the smooth problems such as the one discussed in Section 5.1 the DD, WDD and $\text{DG}_{\text{bilinear}}$ methods seem to have comparable convergence rates. The lower computational costs would suggest

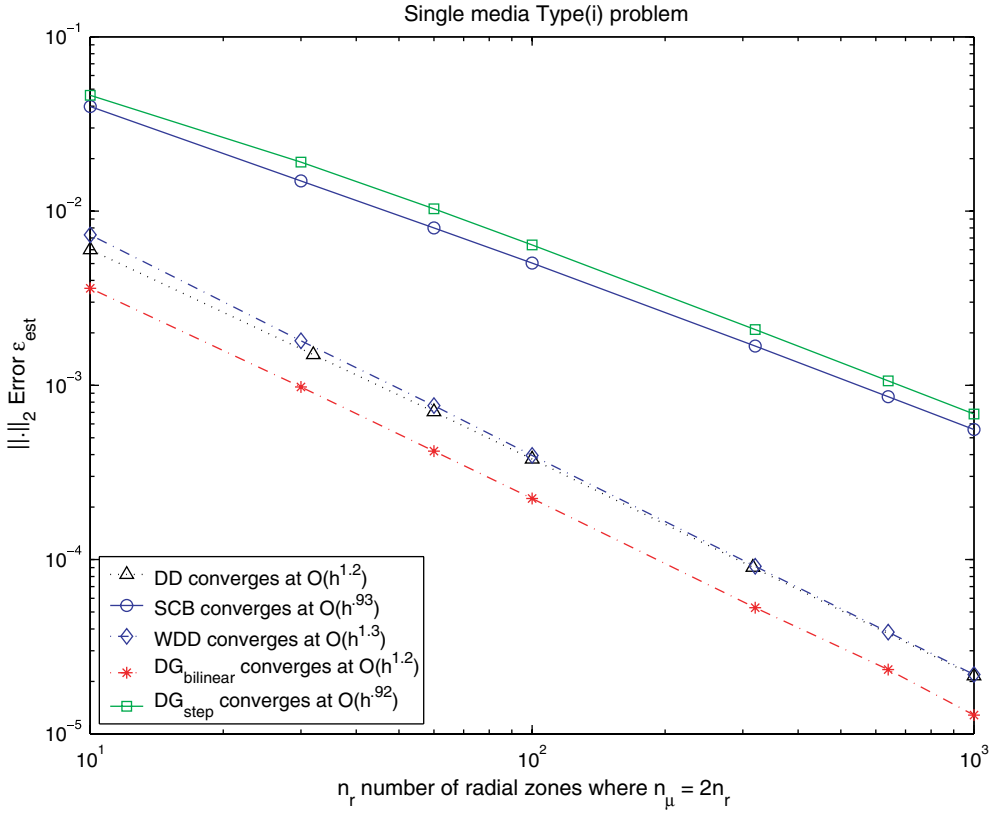

Fig. 6.2. $\|.\|_2$ error ε_{est} in ψ for Type (i) problem as function of number of radial zones. Horizontal axis is n_r. Here the number of angular zones is exactly twice the number of radial zones: $n_\mu = 2n_r$. Also $h = \frac{1}{n_r}$. See Section 1.2 for details on the mesh shape. The error rates are similar: $O(h^p)$ for $p = .92$ to 1.3. However, the $\text{DG}_{\text{bilinear}}$, DD, and WDD methods have a much lower error than the SCB and DG_{step}.

that the DD and WDD methods might be preferable to DG methods were it not for other numerical properties of interest such as positivity and elimination of the flux-dip.

6.2. Oscillations and positivity

Non-physical oscillations and negativity are well documented problems in numerical differential equations as a whole (e.g. [11]) and for neutron transport in particular [13,18]. Both WDD and DD methods exhibit such non-physical numerical aberrations as is common with classic centered-difference type methods. This is especially common in the presence of strong discontinuities in σ and q such as those posed by the Type (ii) problem in Section 5.2. See Fig. 6.3.

Table 6.1 is a comparison of various DG solutions to the Type (ii) mixed media problem. Again it is interesting to note that in all cases, there are little or no oscillations (see also Fig. 6.4). However under more extreme conditions where $\sigma_2 = 1000$ (as in (5.4)), numerical experiments have revealed that minor oscillations can crop up.

6.3. Flux-dip and other r = 0 inaccuracies

It has been observed in [9,14–17] that the DD method can exhibit non-physical inaccuracies near $r = 0$. A major class of these inaccuracies comes in the form of a "flux-dip". Fig. 6.3 shows that both SCB and DD methods exhibit a flux-dip. It is a complicated effect that involves angular discretization, spatial discretization

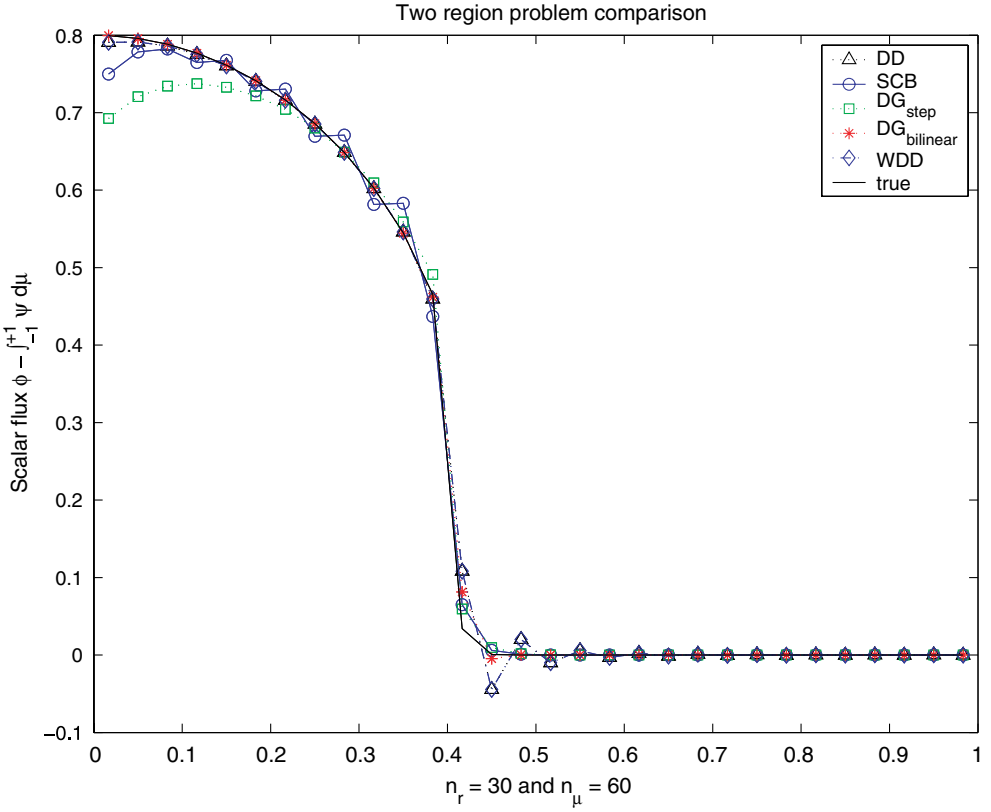

Fig. 6.3. A comparison of scalar flux for Type (ii) mixed-media problem. The 'quasi-exact' nature of the solution comes from applying a quadrature approximation to the exact neutron flux ψ_{exact} yielding $\phi(r_i) = \sum_{d=1}^{d=n_d} \psi_{\text{exact}}(r_i, \mu_d)\Delta\mu_d$. Note the flux 'dip' near $r = 0$ for some methods, and the oscillations that can occur with others at $r = .4$. Here, as elsewhere if not stated otherwise $n_\mu = 2n_r = 40$.

Table 6.1
Comparison of various DG methods on Type (ii) two-media test problem described in Section 5.2

Trial/test space $K_{i,d}$	Oscillations near $r = .4$	Dip at $r = 0$	Error rate[a] $h = \frac{1}{n_r}$	
span$\{1\}$	No	Yes	$h^{.69}$	DG_{step}
span$\{1,\mu\}$	No	Yes	$h^{.72}$	$DG_{\mu\text{-linear}}$
span$\{1,r\}$	No	Yes	$h^{1.1}$	$DG_{r\text{-linear}}$
span$\{1,r,\mu\}$	No	Slight	$h^{1.2}$	
span$\{1,r,\mu,r\mu\}$	No	No	$h^{1.2}$	$DG_{bilinear}$
span$\{1,r,\mu,r\mu,\mu^2,r^2\}$	No	No	$h^{1.3}$	$DG_{quadratic}$
span$\{1,r,r^2\}$	No	Yes	$h^{1.0}$	
span$\{1,\mu,\mu^2\}$	No	Yes	$h^{.72}$	
span$\{1,\mu,r\mu\}$	No	Yes	$h^{.72}$	
span$\{1,\mu,r\mu,\mu^2\}$	No	Yes	$h^{.72}$	
span$\{1,\mu,\mu^2,\mu^3\}$	No	Yes	$h^{.72}$	

[a] By comparison, the DD and WDD methods converged at $O(h^{1.2})$ and SCB converged at $O(h^{.76})$ for the same problem with a slightly different mesh. See Section 1.2 for differences in mesh.

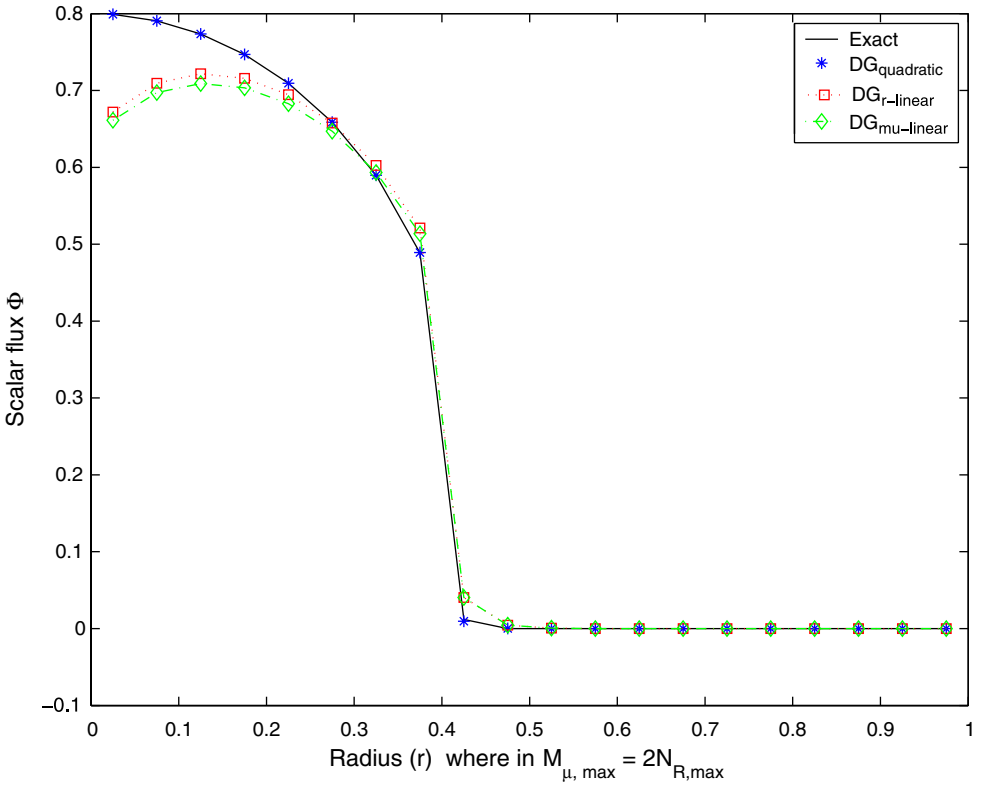

Fig. 6.4. A comparison of scalar flux for the Type (ii) mixed media problem estimated with DG methods using some of the possible test and trial spaces not presented in previous figures – see Table 6.1. Note that in all these cases, there is little to no oscillation near $r = .4$ regardless of test-space being used. $n_r = 20$ and $n_\mu = 40$.

and boundary conditions at the origin of the sphere. The flux-dip has been studied predominantly in settings where there is a

1. scattering operator term incorporated into the RHS of (1.1),
2. highly refined radial discretization (large n_r), and
3. low angular resolution (small n_μ) coupled with a
4. non-uniform angular discretization such as Gauss–Legendre quadrature.

In an investigation of the DD method, [14] developed a theory of the flux-dip phenomenon in the context of highly diffusive, scattering media. Their results show that flux-dip phenomenon can be ameliorated by substituting the WDD angular discretization (2.4) for (2.3). Interestingly, the WDD-type angle discretization scheme can be incorporated into a variety of other schemes as shown in [17] and elsewhere. Results in Figs. 6.3 and 6.4 show that by including both linear and bilinear terms in the trial and test spaces, the discontinuous Galerkin methods can suitably remove the flux-dip.

In the context of Table 6.1, it should be noted that only lower order methods that lack a linear dependence on both angular and radial variables exhibit a flux-dip. It was observed that the flux-dip can, in many cases, be avoided by simply using a uniform angular discretization. Although discussed in the context of the DD and WDD methods, [14] has a very nice discussion of this phenomenon.

Walters and Morel in [17] noted that the bilinear DG method (which they refer to as the SLD – standard linear discontinuous method) can exhibit a different class of inaccuracies at the origin under conditions #2 and #3 outlined above (highly refined radial mesh, but poorly refined in the angular variable). Compare for example, Fig. 6.5 with Fig.1 of [17]. Walters and Morell speculate this is a result of insufficient starting direction information (incorporating solution data where $\mu = -1$). They offer a modification of $DG_{bilinear}$ that incorporates more starting flux information by the judicious use of continuous, quadratic-in-angle functions along cells that border the $\mu = -1$ domain boundary.

However, results in Fig. 6.5 suggest that considerable improvement can be made in the solution's behavior at the origin by simply including a quadratic (μ^2) term in either the linear or bilinear DG method, neither of which use starting direction information (see in particular the bilinear hybrid method in Fig. 6.5). Numerical experiments show that comparable improvements are made if along the cells bordering the $\mu = -1$ direction, higher order μ spaces are used, analogous to the idea of [17] but in the discontinuous setting.

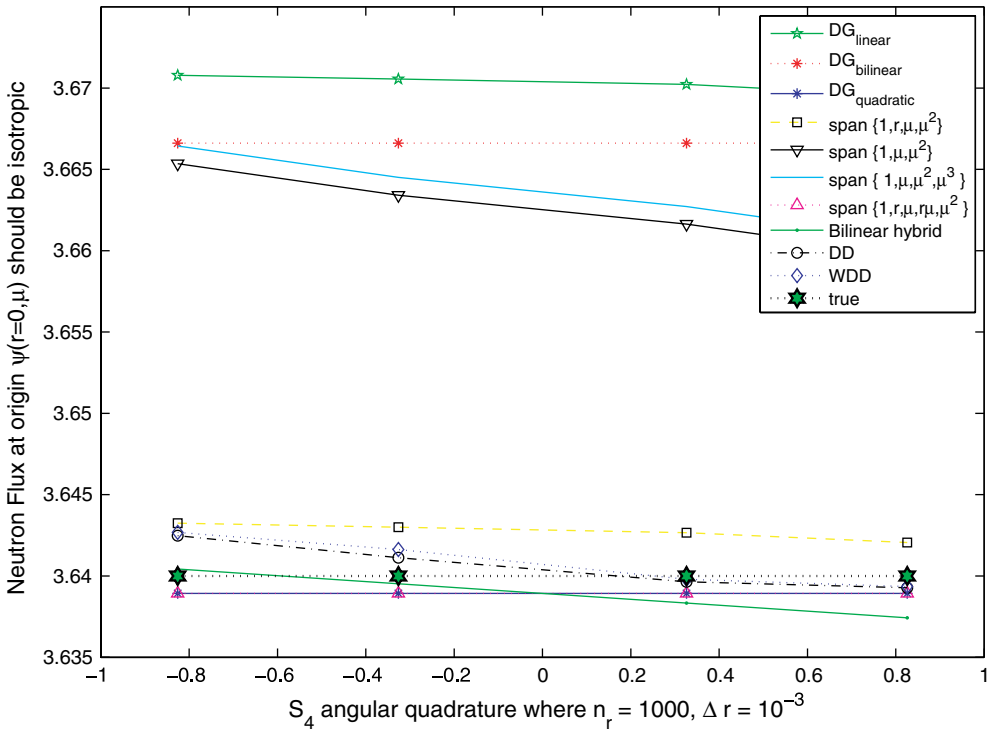

Fig. 6.5. A graph of the neutron flux at the origin using a variety of numerical methods described here. Solution parameters determined by $\sigma \equiv 1$, $q \equiv 0$, and isotropic incoming boundary conditions, such that the true solution at the center is 3.64 independent of μ. The solution is resolved on a mesh with $n_r = 1000$ and $n_\mu = 4$. SCB and DG_{step} are not included in the graph as the results were grossly inaccurate in comparison to the methods presented above with 200–1000% relative errors. The bilinear hybrid method uses μ-quadratic test/trial functions in the cells that abut the $\mu = -1$ boundary, yet uses bilinear test/trial functions otherwise.

Table 7.1
Summary table

Criteria	DD	WDD	SCB	$DG_{Bilinear}$	DG_{Step}
1. Positivity	No	No	Yes	Yes	Yes
2. Avoids 'dip' near $r = 0$	No	Yes	No	Yes	No
3. Convergence rate					
Smooth problem	1.2	1.2	1.1	2.2	.82
Type (i) problem	1.3	1.3	.93	1.2	.92
Type (ii) problem	1.2	1.2	.76	1.2	.69
4. Approx. flops/cell (sub-cells in SCB)	37	37	39	320	19

7. Conclusions

In view of the criteria described in Section 1.1, as long as the DG method includes first order terms in the test and trial spaces, it offers several advantages as can be seen in the summary Table 7.1. In particular, $DG_{bilinear}$ has an all around superior performance when compared to the DD or SCB methods.

The $DG_{bilinear}$ method has very little oscillation or negative flux problems especially when compared with the WDD and DD methods. Although the SCB and the DG_{step} methods maintain strict positivity in the test problems considered, they exhibited other unphysical behaviors and lower rates of convergence.

Furthermore, the $DG_{bilinear}$ method avoids the flux-dip problem that plague some other methods. Lower order discontinuous Galerkin methods such as the DG_{step} are susceptible to the $r = 0$ flux dip problem as are the DD and SCB methods. The WDD's well documented feature is that it avoids the flux-dip problem in most numerical regimes of interest. It should be noted that discontinuous Galerkin methods will tend to have a higher computation cost per cell when compared to other methods. Furthermore, this computation cost increases as higher-order test and trial spaces are used: a $m = \dim K_{i,d}$ dimensional trial space will require an $m \times m$ dense matrix solve for each cell. Generally however, as can be discerned from Figs. 6.1, 6.2, and Table 7.1 the greater accuracy of the $DG_{bilinear}$ can significantly outweigh the increased computational costs.

8. Future work

The opportunity for combining several of the ideas described here is great. For example, combining the SCB method with the idea of a weighted angular-discretization will remove the flux-dip and maintain positivity. Unfortunately, numerical experiments suggest that the poor convergence properties of the SCB method are retained when compared with the $DG_{bilinear}$ method.

Other combinations might prove fruitful. Several authors [9,17] have discussed using a linear discontinuous-type method that incorporates a quadratic-continuous scheme in the first angular cells. Numerical experiments suggest that certain quadratic discontinuous elements (or perhaps other test and trial space combinations) might suffice (i.e. the bilinear hybrid method in Fig. 6.5). This might retain some of the desirable, numerical properties while lowering computational costs per cell. Other (non-linear and/or higher-order) flux-limiting type methods [11] might be incorporated as well under such circumstances. This might even be generalizable to adaptive schemes for picking test/trial spaces.

In the presence of scattering, [15] describes an iterative technique used in highly diffusive conditions in this geometry: Diffusion Synthetic Acceleration. They report excellent performance for some finite element methods but poor performance on others. Numerical experiments conducted on the $DG_{bilinear}$ seem to show some promise when compared to *DD* methods, but a more detailed effort is required to more fully understand its convergence properties.

Acknowledgments

I would like to especially thank Prof. A. Greenbaum for her longstanding support, encouragement and patience. I would also like to thank Dr. B. Chang for his mentorship and support during my time at LLNL. Thank you both.

References

[1] R.T. Ackroyd, W.E. Wilson, Discontinuous finite elements for neutron transport analysis, Progr. Nucl. Energy 18 (1–2) (1986) 39–44.
[2] M.L. Adams, A new transport discretization scheme for arbitrary spatial meshes in XY geometry In: Proceedings of the International Topl. Mtg. Advances in Mathematics, Computations, and Reactor Physics Pittsburgh, Pennsylvania, April 28–May 2, 1991, vol. III, American Nuclear Society, 1991, p. 13.2 2-1.
[3] M.L. Adams, Sub-cell balance methods for radiative transfer on arbitrary grids, Transp. Theory Stat. Phys. 26 (1997) 385–431.
[4] M. Asadzadeh, A finite element method for the neutron transport equation in an infinite cylindrical domain, SIAM J. Numer. Anal. 35 (1998) 1299–1314.
[5] B.G. Carlson, K.D. Lathrop, Transport theory the method of discrete ordinates, in: H. Greenspan, C.N. Kelber, D. Okrent (Eds.), Computing Methods in Reactor Physics, Gordon and Breach, New York, 1968, pp. 167–266.
[6] B. Cockburn, G.E. Karniadakis, C.-W. Shu (Eds.), Discontinuous Galerkin Methods Theory, Computation and Applications, Springer-Verlag, Heidleberg, 2000.
[7] A. Greenbaum, J.M. Ferguson, A Petrov–Galerkin finite element for solving the neutron transport equation, J. Comput. Phys. 64 (1986) 97–111.
[8] C. Johnson, Numerical Solution to Partial Differential Equations by the Finite Element Method, University of Cambridge Press, New York, 1987.
[9] K.D. Lathrop, A comparison of angular difference schemes for one-dimensional spherical geometry s_n equations, Nucl. Sci. Eng. 134 (2000) 239–264.
[10] P. Lesaint, P.-A. Ravaint, On a finite element method for solving the neutron transport equation, in: C. de Boor (Ed.), Mathematical Aspects of Finite Elements in Partial Differential Equations, Academic Press, NY, 1974.
[11] R.J. Leveque, Numerical Methods for Conservation Laws, Birkhäuser Verlag, Basel, 1992.
[12] E.E. Lewis, W.F. Miller, Computational Methods of Neutron Transport, John Wiley, New York, 1984.
[13] K.A. Mathews, On the propagation of rays in discrete ordinates, Nucl. Sci. Eng. 132 (1999) 155–180.
[14] J.E. Morel, G.R. Montry, Analysis and elimination of the discrete-ordinates flux dip, Trans. Theory Stat. Phys. 13 (5) (1984) 615–633.
[15] T.S. Palmer, M.L. Adams, Analysis of spherical geometry finite element transport solutions in the thick diffusion limit in: Proceedings of the International Topl. Mtg. Advances in Mathematics, Computations, and Reactor Physics Pittsburgh, Pennsylvania, April 28–May 2, 1991, vol. V, American Nuclear Society, 1991, pp. 21.1 3-1–21.1 3-15.
[16] T.S. Palmer, M.L. Adams, Curvilinear geometry transport discretization in the "thick" diffusion limit, in: Proceedings of the International Conference Math. Methods & Supercomputing in Nuc. Appl., Karlsrühe, Germany 4/19-4/23, vol. I. Kernforschungszentrum, Karlsrühe, 1993, p. 33.
[17] W.F. Walters, J.E. Morel, Investigation of linear-discontinuous angular differencing for the 1-D spherical geometry SN equations (U)Proceedings of the International Topl. Mtg. Advances in Mathematics, Computations, and Reactor Physics Pittsburgh, Pennsylvania, April 28–May 2, 1991, vol. III, American Nuclear Society, 1991, p. 13.2 3-1.
[18] W.F. Walters, T.A. Wareing, An accurate, strictly-positive, nonlinear characteristic scheme for the discrete-ordinate equations, Trans. Theory Stat. Phys. 25 (2) (1996) 197.